Invited Paper

Design, Fabrication and RF Testing of Near-THz Sheet Beam TWTA

Anisullah Baig Student Member, IEEE *, Young-Min Shin, Larry R. Barnett, Diana Gamzina, Robert Barchfeld, Calvin W. Domier, Jianxun Wang, and Neville C. Luhmann Jr., Fellow IEEE
Department of Electrical and Computer Engineering, University of California – Davis, CA 95616, USA
* Email: abaig@ucdavis.edu, anis.ucd@gmail.com

(Received September 16, 2011)

Abstract: There is increasing realization that the region of electromagnetic spectrum between 100 *GHz*-1 *THz* has a myriad of potential applications that could directly impact society. These include security applications like non-invasive detection of concealed weapons, explosives and contraband items; imaging of thermonuclear fusion plasmas, medical imaging or detection of cancer, industrial quality control, and future ultra-wide band/high data rate communication systems. For the quest for high frequency and high power sources required to realize these applications and close the so-called THz gap, microwave vacuum integrated technology is an extremely attractive choice for their ability to handle high power in a relatively compact volume. However, the beam-wave interaction physics imposes constraints on the fabrication tolerances and surface roughness that an RF structure can possess. This directly impacts the cold (RF transmission only) and hot (beam and RF interaction) characteristics/performance of the tube. Thus, as we proceed to frequencies in the THz region, conventional machining is unable to handle the required structure fidelity and surface quality.

In this paper, our efforts involving the design, fabrication and RF measurements of an 0.22 *THz* ultra wide band sheet beam travelling wave tube amplifier are described. Eigen mode dispersion curve analysis and particle-in-cell analysis of the UC Davis designed TWT demonstrated wide band width (> 50 *GHz*; i.e., ~ 30% instantaneous BW). The output power was calculated to be > 50 *W* in the pass band for an input drive of 1 *W*. A PPM based sheet beam transport focusing structure employing $SmCo_6$ magnets and an existing sheet electron gun developed by CPI [1]for use in a proof-of-principle experiment is also described that showed a beam transmission of 80 % that corresponds to a transmitted current of ~ 207 *mA* for a 20 *kV* electron beam.

We also describe MEMS fabrication technology to make micro-metallic structures/waveguides possessing the requisite high dimensional definition and low surface roughness (< skin depth). Our efforts in MEMS precision fabrication have primarily focused on the following areas: (a) LIGA technique for high aspect ratio structures in a single process employing KMPR[2, 3] and SU-8[2, 3]; (b) Si-DRIE process[4]; and (C) Nano-machining / nano-CNC milling[5]. We were successful in fabricating completely metalized 0.22 *THz* TWTA circuits within 3-5 μm tolerance and a surface roughness ranging from 30-80 *nm*. An extensive SEM and 3D microscope analysis was also conducted and described in detail. A scalar network analyzer system was configured for RF measurements employing a BWO in the frequency range 180-265 GHz^2. Both KMPR LIGA and nano- machined circuits showed an excellent agreement with the simulations with S_{21} ~ -5 *dB* in the passband and also matching well the predicted 1 *dB* bandwidth of ~ 65 *GHz* predicted from 3D FDTD and FEM electromagnetic solvers. S_{11} remained a little high for the case of LIGA circuits as compared to the simulated value of ~ -10 *dB*, but for the nano machined circuits S_{11} gave an excellent agreement with the simulation.

We also describe in this paper our idea/preparation for an exploratory proof-of-principle hot test employing MEMS fabricated TWTA circuits. The PIC analysis for MEMS fabricated circuits placed in a holder assembly that connects an existing sheet beam electron gun, PPM structure, vacuum ports and input/output couplers suggested an output power of ~ 70 *W* for an input drive of ~ 1 *W* at 0.22 *THz*.

It is hoped that MEMS fabricated micro-scale vacuum electron devices will pave the way for the elimination of the so-called "THz gap" by scaling for high frequency operation. This is also important for many applications in the THz region that demands compact and mobile device with reasonable power and bandwidth.

Keywords: MEMS Fabrication, Vacuum Electron Devices, THz Gap, LIGA Fabrication, Nano-Milling/Machining, Vacuum integrated Power Amplifiers, MM-Wave/THz Technology

doi: 10.11906/TST.181-207.2011.12.24

1. Introduction

THz electromagnetic radiation in the region 0.1-1 *THz* [7, 8] falls between the so-called electronics and photonics areas of research as shown in Fig. 1 It has gained considerable attention in the last few years due to attractive features [9] including (a) penetration through most non-metallic materials, (b) non-ionizing as compared to X-rays, (c) penetration dependent upon water concentration and tissue densities, and (d) wide bandwidth possibility at these high frequencies.

Between 1-100 *GHz*, the maximum achievable output power of both solid state sources and vacuum electron devices (VEDs) scales as ~ f^2 [10]. This is related to scaling of lateral dimensions of the slow wave circuit dimensions with the wavelength corresponding to the operating frequency. However, this power versus frequency scaling ($P \sim f^2$) of electromagnetic sources no longer holds for frequencies > 100 *GHz* as shown by the dashed part of the green line in Fig. 1 This gives rise to what is known as the 'THz gap' of adequately powerful source technologies for coherent electromagnetic radiation.

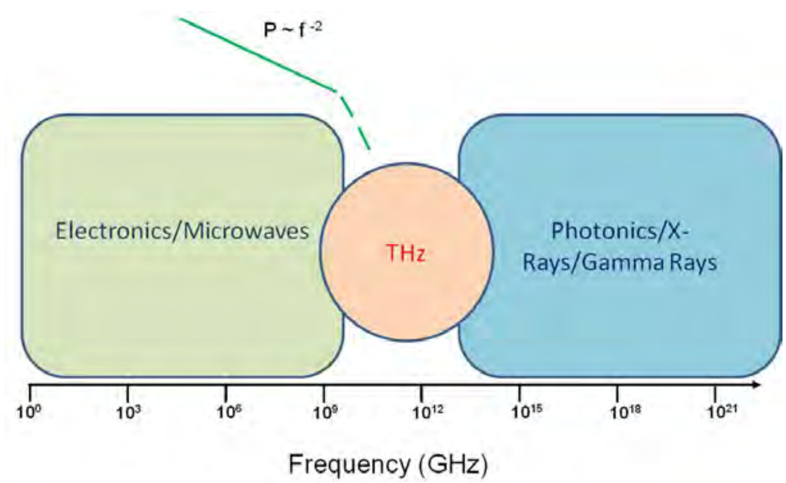

Fig. 1 The THz regime 100 *GHz*-1 *THz* and beyond lies in between the electronics and photonics area of research. The green line emphasizes the sharp drop in output power ($P \sim f^2$ scaling no longer holds) observed for both solid state and vacuum based compact microwave devices in the THz region.

The term "THz gap" is commonly employed in current literature [7, 8] to describe the fact that despite substantial applications, there has been a lack of available source technology with reasonable power in a compact volume package. This has generated considerable interest in the scientific community to realize the sources for a number of proposed important applications [11-

15] ranging from industrial quality control, non-protrusive contra-band item detection, medical imaging/cancer diagnostics, all weather visibility systems for aviation safety, advanced telecommunication systems and radar with high wireless data transfer rates for LPI (low probability of interception), and commercial applications.

All these applications demand reasonable output power [10] (*CW*) from 0.01 *W* to tens of Watts in a mobile device working in THz frequencies with an intrinsic efficiency of > 1% and a typical required instantaneous bandwidth of $\gtrsim$ 1%. At high frequencies, however, in the THz gap power decreases more rapidly than f^2. Hence, it becomes more challenging as we move toward the demand for more power at high frequencies.

Solid state sources are known to have heat management and break down issues for high power at high frequencies[16]. The highest average powers for solid state sources at $f \geq 1$ *THz* include ~ 10 μW nonlinear multiplier sources above 1 *THz* [17] and milli-watts at several THz using either quantum cascade lasers [18] or difference frequency mixing. It is challenging to achieve significant power from quantum electronic devices as they require cryogenic cooling to suppress thermal broadening disrupting population inversions.

There also has been considerable work on coherent radiation generation in the THz regime [17-21] namely FELs such as those at Novosibirsk and, Jefferson Lab and Fast Wave Devices/Gyrotrons. However, none of the above represents a compact, mobile device. Nevertheless, vacuum based coherent radiation generation/source technology has an advantage that electrons move 'freely' in the beam tunnel under high vacuum interacting with the co-propagating electromagnetic radiation under the influence of electric and magnetic fields. This is advantageous to obtain high powers while still managing parasitic heat dissipation. After the beam-wave energy transfer reaches saturation in the device, there are separate channels for spent electron beam collection and THz radiation propagation. This also enhances the capability to design efficient channels for maximizing RF power and minimizing dissipated heat in the system.

There are also some fundamental differences in a solid state and vacuum electronic device. In a vacuum device, the electron beam flow in vacuum is collisionless, while in a solid state device the collision-dominated stream diffuses through a semi-conducting solid. Thus, a solid state device is unable to conduct away excessive heat generated by the electron current in the interaction region. Moreover, there is a high probability of a dielectric breakdown at high microwave field strengths. These limitations do not exist at least to this high degree as in solid state devices. Furthermore, the efficiency of a vacuum electron device can be enhanced by using energy recovery mechanism or a multistage depressed collector[22]. Thus, for achieving reasonable power in a compact sized package at THz frequencies, vacuum integrated power amplifier (VIPA) technology is a superior choice [23-26].

2. TWTA Design: eigen mode analysis (dispersion curve) and PIC analysis

Traveling wave tube amplifiers (TWTAs) attract considerable attention [23-25] for use as high power THz amplifiers, as they have moderate beam-wave energy conversion efficiency, moderate to high instantaneous bandwidth and large RF thermal capacity. In THz MPM (microwave power module) type applications, planar circuit structures [27] are advantageous over round ones as their efficiency is proportional to beam wave interaction area. Increasing the aspect ratio of the electron beam also reduces the space charge forces and hence allows compact magnetic focusing structures employing permanent magnet technology. Furthermore, novel MEMS (Micro-Electro-Mechanical System) fabrication schemes can be employed relatively easily for planar structures.

In our group, a novel 0.22 *THz* traveling wave tube amplifier design was conceived [28-30] for modern communication and sensing applications. It consists of a staggered double-vane grating array operating in the TE-mode. The full TWT simulation model of ~ 40 *mm* length with integrated broad band tapered vane couplers is shown in Fig. 2 (a). The inset shows a single period eigen-mode analysis model with a period of 460 μm, beam tunnel height of 150 μm, vane depth of 270 μm, and beam tunnel width of 770 μm. The longitudinal field components with in-phase symmetry between corresponding vane inner edges is also shown that enhances the energy conversion from the electron beam to the THz electromagnetic waves. This phase-shift between two TE-mode gratings also provides an ultra wide band width amplification attributed to the presence of effective surface plasmons (ESPs) in the beam tunnel. Fig. 2 (b) shows the FDTD eigen-mode solver simulation for the dispersion curve of the single cell of TWT amplifier circuit. The 20*kV* beam line is also plotted that clearly shows the broadband velocity synchronism condition for the n = 1 mode and centered at $k_z d/\pi = 2.5$ around 0.22 *THz*. Fig. 2 (c) shows that the Particle-in-Cell analysis codes MAGIC and CST match very well in describing the gain versus frequency response of the TWTA. The 3 *dB* band width was calculated to be ~ 66 *GHz* which corresponds to ~ 30 % instantaneous band width at 0.22 *THz*.

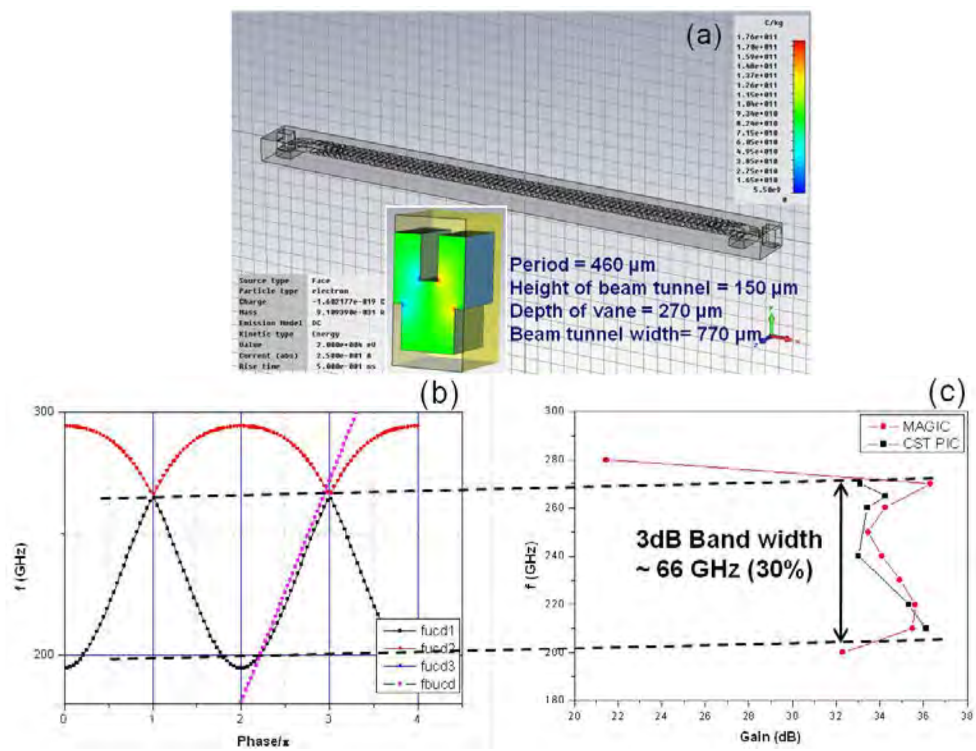

Fig. 2 (a) 40 *mm* TWT circuit model with integrated broadband tapered vane couplers; inset shows single cell for 3D EM eigenmode analysis (b) Dispersion curve and spatial harmonics for modes n = 1 and n = 2. (c) Gain versus frequency curve to show the broadband velocity synchronism and amplification with ~ 30 % 3*dB* band width at 0.22 *THz*.

The TWT output response was studied using particle-in-cell simulation codes, namely the MAGIC and CST PIC codes. The input setting was an electron beam of 20 *kV* and 250 *mA*, and an RF drive at 0.22 *THz* of power 50 *mW* for annealed copper as the slow wave structure wall material. For this device performance analysis, an analytic B-field of 2 Tesla was defined in the simulation setup. For a more realistic analysis, a PPM based sheet beam focusing structure was also designed and studied in PIC simulations that will be described in a later section. The output response from both PIC codes is described in Fig. 3.

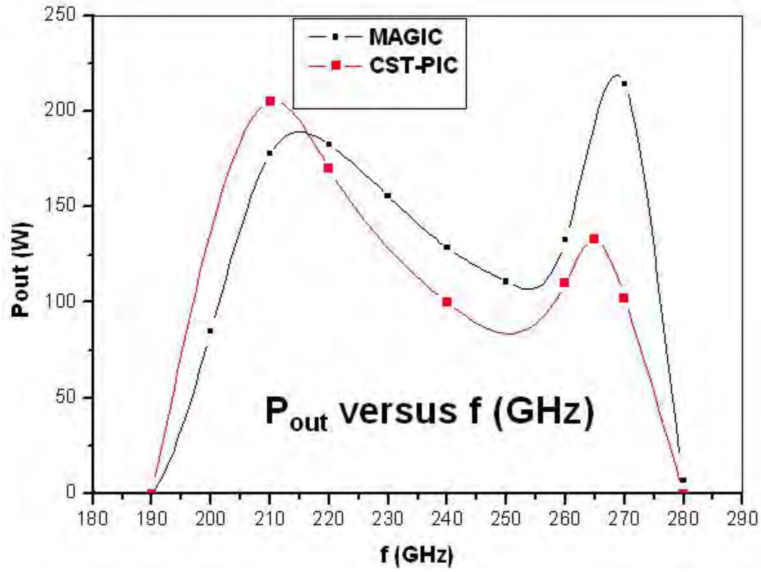

Fig. 3 Particle-in-cell (PIC) analysis for TWTA using the MAGIC and CST PIC codes

The output response correlates well with the eigenmode solution and FDTD simulation/S-parameters simulation of the TWT circuit. The output power lower cutoff is around 190 *GHz* and the upper cut off is ~ 280 *GHz*. Between these frequencies, the TWT demonstrates wide band amplification of > 50 *W*. The peak in output power versus frequency response at around 265 *GHz* is being studied further to investigate the possible existence of high order mode parasitic oscillations. A MEMS compatible sever design is also being integrated into the PIC simulation modeling for the stability of the wide band traveling wave tube amplifier.

2.1 Sheet beam transport (PPM design, beam transmission)

In the mm-wave frequency region of the electromagnetic spectrum, the current density requirement for the beam-wave interaction increases as the square of the frequency [31], so it becomes very difficult to design a magnetic focusing mechanism for a single cylindrical beam due to excessive space charge effects. This also prevents the device from operating at relatively high powers. In addition, it requires high magnetic fields that cannot be provided by permanent magnets. For a compact and portable device, there has been considerable interest in the use of multiple beams [32]. A sheet beam configuration[33] is also a collection of several small scale beamlets, but it is relatively easier to start from a circular cathode and with a focus electrode design and appropriate biasing so that the beam can be shaped into an elliptical shape. By spreading the beam in one direction, we can transport more current (hence more power) while still keeping the same gun perveance. Periodic Permanent Magnetic (PPM) focusing has been studied extensively [34-36] for its application in sheet beam transport for a compact high power microwave/millimeter wave VED. For our SBTWTA, we designed a PPM based focusing structure[37] to efficiently transfer the elliptical beam through an ~ 40 *mm* beam tunnel. The simulation model is shown in Fig. 4 (a). The axial B-field varies periodically as shown in Fig. 4 (b).

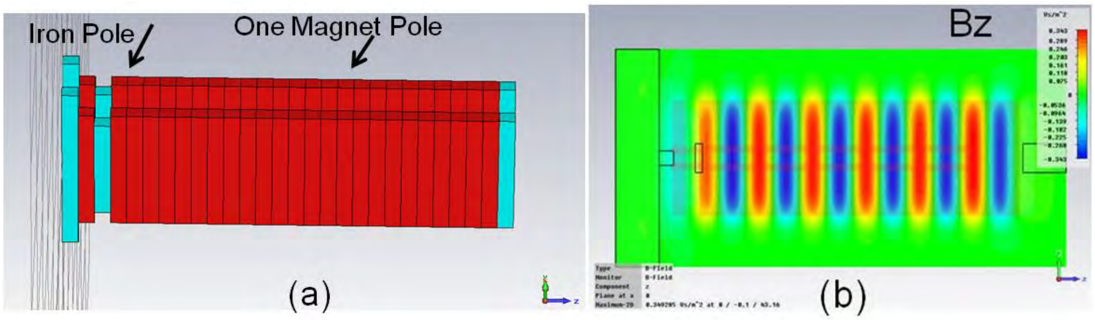

Fig. 4 (a) Periodic Permanent Magnet (PPM) sheet beam focusing model (b) contour plot of periodically varying axial B-field

We plan to utilize an available sheet beam gun [1] operating at 20 *kV* and providing a current of 416.2 *mA* which was employed in early proof-of-principle beam formation and transport studies[38]. The sheet beam aspect ratio from this gun is higher than that required by our interaction structure, so an aperture is modeled just after the gun assembly that houses the slow wave structure. The current provided by the source is 416.2 *mA* which is cut down to about 259 *mA* after which it enters into the beam tunnel as shown in Fig. 5 (a). The current PPM design for the first simple proof-of-principle test transports this current with 80% beam transmission for the assumed 2.6 *mm* spacing between magnet stacks for $SmCo_6$ permanent magnets as shown in Fig. 5 (b)[1]. To ease the precision fabrication of vacuum ports that extends perpendicular from the narrow dimensions of the tube, it is needed to increase the stack to stack spacing from 2.6 *mm*. We worked on relatively high remanence magnetization permanent magnets i.e NdFeB. The initial results were promising and we obtained ~ 73% beam transmission that corresponds to a transmitted current of ~ 190 *mA* with an increased spacing of ~ 4 *mm* between magnet stacks. The work is underway to further optimize the sheet beam focusing structure to maximize electron beam transmission.

[1] We note that this proof-of-principle test system is not optimized and that we have obtained better than 99 % transmission in our W-Band Sheet Beam Klystron (WSBK) experiments

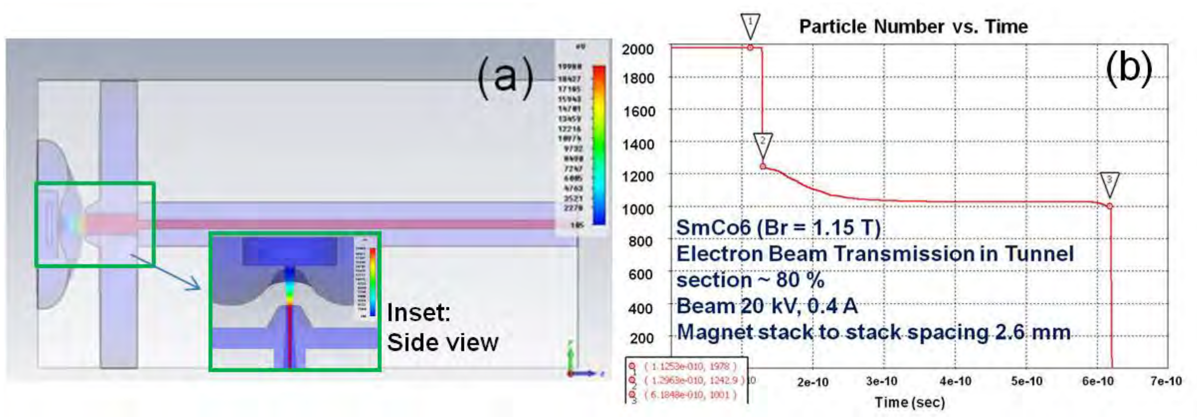

Fig. 5 Sheet beam transmission in 770 μm * 150 μm tunnel employing UCD designed PPM structure (b) simulation result showing 80% transmission in the beam tunnel using $SmCo_6$ permanent magnets with a stack spacing of 2.6 *cm*

2.2 Exploratory hot test preparation

We have accomplished simulation modeling and fabrication of all the key aspects for an exploratory hot pulsed test of the 0.22 *THz* SBTWTA with a bandwidth of > 50 *GHz* and ~ 50 *W* output power. For the initial proof of principle test, our experimental target is to achieve 500 *W-GHz* power bandwidth product. The basic idea is to utilize the UV LIGA and Nano Machined fabricated slow wave structures placed in a specially aligned fixture that houses the electron gun/cathode assembly with the integrated input/output couplers. The PPM based magnetic focusing structure sits parallel to the sheet beam while vacuum ports are in the lateral/narrow dimension. A schematic for the exploratory hot test assembly is provided in Fig. 6. The RF output section is a coupler/collector hybrid design to be used as an RF extraction channel as well as spent beam dump. It is important to note that this proof-of-principle study will be conducted pulsed at low duty and hence does not require a water cooled high thermal capacity collector. The optimization of the structure was conducted both from the perspective of efficient millimeter-wave transmission and a gradual electron beam interception before the RF output window.

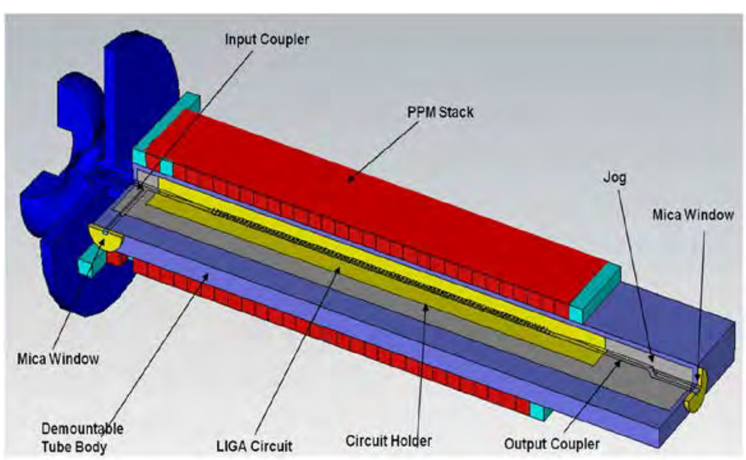

Fig. 6 Schematic for the exploratory hot test assembly with LIGA and nano machined circuit and integrated input couplers and output coupler/collector hybrid. PPM stack and electron gun/cathode assembly is also labeled.

Particle-in-cell (PIC) simulations were conducted to analyze the TWT performance with the designed PPM B-Field. The PPM B-field was integrated into the simulation setup with emission imitating the position of the cathode in the gun assembly with respect to the magnet stack. The power flow in the simulation was observed to be maximized near the output port clearly demonstrating the beam-wave interaction for RF amplification for a 10 nsec simulation. The reflective time scale of the electromagnetic wave interacting with 20 *kV* electron beam (slow space charge wave) is of the order of ~ 1 *nsec*. This timescale is important to identify if there is some sort of instability in the output response (fluctuation repetition) attributed to the amplification of a reflected wave typically in a sever-less circuit. The beam is defined with 20 *kV* and 190 *mA* current as dictated by the beam transmission simulation using CST PS after optimizing the PPM magnet design for a stack spacing of 4 *mm* using NdFeB magnets. Fig. 7 (a) shows the beam wave modeling simulation result for the 190 *mA* (73% beam transmission case) using the PPM B- field employing NdFeB permanent magnets and a realistic stack spacing of 4 *mm*. For an input drive of 1 *W*, an output power of 70 *W* is predicted with a gain of 18.45 *dB* and 1.4% electronic efficiency. The reflected power recorded at port 1 is 1.8 *W*. This reflected power can damage the RF input driver and hence a sever design is underway to minimize the reflections in the system and enhancement of efficiency. Fig. 7 (b) shows the FFT amplitude of the input, output and, reflected signals and we see a most prominent peak at 220 *GHz* (frequency of the input drive). This demonstrates the stability of device operation and absence of parasitic tube oscillation at higher frequencies.

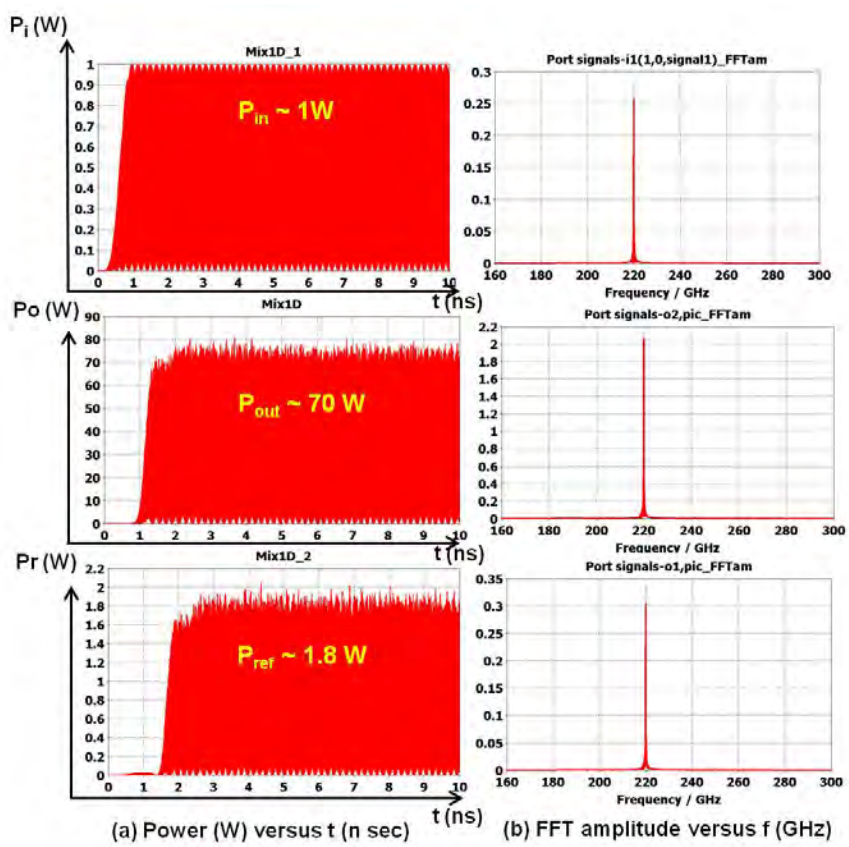

Fig. 7 (a) Output power of TWT in PIC analysis giving ~ 70 *W* for an input of 1 W at 0.22 *THz*. (b) FFT analysis showing spectral purity and fundamental mode amplification at 0.22 *THz*.

3. Fabrication

To realize a compact and reasonable power device in the THz regime of the electromagnetic spectrum, the transverse dimensions of the cavity or slow wave structure scale down to ~ 0.1 λ_0 (~ 100 μm at 300 *GHz*) [39-41]. Moreover, stringent fabrication tolerance (typically < 10%) is required for metallic microstructures while simultaneously constraining surface roughness to be less than the skin depth at the operating frequency [5]. Therefore, conventional machining technology was unable to meet the specifications needed to precision manufacture the cavity, slow wave structure, electron gun, and cathodes.

To provide a perspective, Fig. 8 (a, b) shows the frequency scaling of slot width and slot depth of the UCD designed double vane half-period staggered grating type SBTWTA [28-30] slow wave structure up to 1 *THz*. For the fabrication of a vacuum integrated power amplifier with THz operating frequency where the grating dimensions reach of the order of ~ 75 μm and surface roughness required at least less than the skin depth (140 *nm* at 0.22 *GHz*), it is important to analyze and compare the fabrication regimes of different relevant technologies.

It is clear that at THz frequencies, conventional machining is unable to fabricate the sub-mm dimensions. Moreover, the real challenge is to fabricate structures with narrow cavity widths but shallower depths that we describe as High Aspect Ratio Structures (HARS).

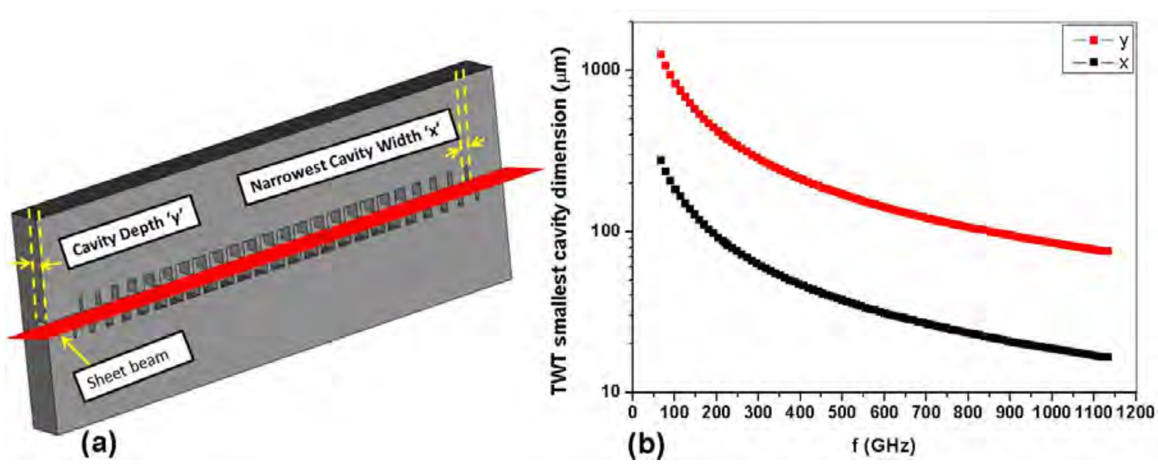

Fig. 8 (a) Double-vane half period staggered 0.22 *THz* Sheet Seam TWT (SBTWT) micro metallic structure (b) narrowest cavity width 'x' and cavity depth 'y' are shown with frequency scaling up to ~ 1 *THz*.

In the last decade, with the advent of the so-called MEMS (Micro-Electro-Mechanical-Systems) technology, it was made possible to potentially bridge the so called "THz gap" and to fabricate the microstructures [42-45] needed for micro-vacuum-electron-devices (μVEDs) with high precision.

Conventional machining is widely used to make various components for microwave devices. Not only there is a variety of machining equipment available, but also there is considerable knowledge that is accumulated about parameters necessary to achieve desired results. For example, Stanford Linear Accelerator Center (SLAC) in collaboration with UC Davis (UCD) used conventional machining techniques to make a W-band sheet beam klystron (WSBK) circuit

[46-48]. Since the machine shop that SLAC and UCD used had enormous amount of experience machining lower frequency components, they already knew how to achieve the best surface finishes and accuracy using the machines they have – all they needed was a smaller set of cutting tools. However, for the klystron to work properly, the circuit needed to be machined with ±1 micron tolerances. This is extremely difficult given that temperature variation in the room that machine is located at causes the parts and the tool to expand or contract more than 1 micron just over a 24 hour period.

The machining technology is moving forward and there are more and more machines that can hold the tolerances needed for the sheet beam klystron, but the machines are expensive and therefore not widely available. However, UC Davis recently initiated a collaboration with Digital Technology Laboratory (DTL) located in Davis, CA. DTL has developed a Nano-CNC milling machine (Mori Seiki NN1000) and allowed UC Davis researchers to use one of their early prototypes to make some of the components for a 220 *GHz* wide bandwidth TWT. In this case, the requirement for the tolerances was also ± 1 micron, but the size of the smallest feature in the circuit was 115 *microns* (compared to ~500 *microns* in the W-band klystron) and the required surface finish was <100 *nm* Ra. Machining technologies like the one developed by DTL are bridging the gap between conventional machining and micro-processing techniques (like the ones used to make computer chips). The size of the features in the components designed to bridge the THz gap falls right in between the capabilities of the two well developed manufacturing techniques – conventional machining and micro-processing.

Electric discharge machining (EDM) is going through a very similar transition as conventional machining: it was disregarded as an option for machining high-frequency components mainly due to the poor surface finish that is formed by the electric discharge, but recently there has been some advancement in the EDM technologies and the machines that are available (i.e., the nano precision wire Sodick EXC100L and sinker AE05 EDM) can make features that are as small as 10 *microns* holding tolerances of less than one micron and achieving surface finishes of up to 10 *nm* Ra.

Tab. 1 provides a table that can be used as a guide when considering a manufacturing technique. It should be noted that the achievable accuracy column refers to the accuracy that can be achieved when making high-frequency components and not necessarily what has been achieved when making different kinds of parts using a given technique. For example, one could achieve nanometer range accuracy with UV LIGA if making micro electro mechanical systems that range from nanometers to few microns in size. Mainly this is due to the fact that the photoresist mold becomes less rigid as its size falls in the hundred's of microns range (THz gap range).

In addition to a specific manufacturing technique that would be used to make a high frequency component, one should also consider other factors – manufacturing design, material choice, and the tooling.

Tab. 1 Table for the comparison of different fabrication techniques and capability, achievable accuracy, and typical surface comparison

Fabrication Technique	Typical capability range	Achievable Accuracy	Typical Surface Roughness
Conventional Machining	> 300 µm	± 5 µm	≥ 200 nm
EDM	80 µm – 1000 µm	± 5 µm	≥ 5 µm
UV LIGA	10 µm – 1000 µm	± 5 µm	≥ 30 nm
DRIE	10 µm – 500 µm	± 1 µm	≥ 30 nm
Nano wire EDM	> 2 µm	± 10 nm	≥ 300 nm
Nano-CNC Milling	> 10 µm	± 0.5 µm	≥ 10 nm

MEMS fabrication technology encompasses a variety of processes, equipment and techniques. In this paper, we will focus on the processes and technologies that were used and are being used successfully specifically from the perspective of progress in µVED device development in the THz regime.

3.1 UV-LIGA

Conventionally, there have been efforts to use synchrotron radiation sources (X-rays) for photolithographic processes [49] including electroforming and mold removal processing. X-rays are significantly penetrable (> 1 *mm*) in the PMMA (polymethylmethacrylate) photoresist and hence have been studied for the realization of mm-wave band micro-vacuum electronic devices. The X-ray LIGA process required beam line time and the entire experiment has to be done at the synchrotron radiation facility which is not always easy. With the advent of new commercially available photoresists, SU-8[50] and KMPR [51] there have been considerable efforts [2, 52] in MEMS fabrication of miniaturized vacuum electron devices using the UV-LIGA process. Fig. 9 shows the typical class-100 clean room equipment required for the UV-LIGA process.

Fig. 9 Typical class-100 clean room equipment for UV LIGA lithography.

3.1.1 SU-8 LIGA

SU-8 [50] is a negative tone photoresist that has a good penetration depth at the i-line (λ = 385 *nm*). The high transparency of this polymer to UV light allows thick molds of the order of ~ 1 *mm*. This enables the lithography to be done in a small clean room facility that is usually dedicated to semiconductor device research and development. This gained significant interest from the scientific community [52-54] to use a UV sensitive negative tone photoresist for the MEMS fabrication of micro-metalized structures for sub millimeter scale vacuum devices. The high absorbency enables one to make high aspect ratio structures; however, it has been established that it is extremely difficult to remove the SU-8 mold from metalized samples after finishing the electroforming and polishing step. There have been numerous efforts for SU-8 removal for example employing reactive ion etching, molten salt baths, water jetting, laser ablation, etc. to efficiently remove SU-8 from the RF channel [55]. Some of these methods require high temperature processes like high temperature ashing; however, the slow wave structure undergoes thermal stress and dimensional changes, hence electroplating quality and surface roughness can be badly affected. Recently, there have been some significant progress in SU-8 removal [52, 56, 57] that can potentially pave the way for more robust and dimensionally accurate high aspect ratio structures.

We worked on two different topologies to use SU-8 for the fabrication of slow wave structures of the 0.22 *THz* SBTWTA: (a) To make two circuit halves made of SU-8 with the empty millimeter wave double vane staggered grating for metal deposition; and (b) To make a negative pattern and mold sits in the RF channel and electroforming is used to cover one circuit half.

Fig. 10 shows an SU8 mold fabricated for metal deposition. SEM analysis showed high definition structures within 1-2 μm fabrication offset and side wall verticality within $\pm 1^{0}$.

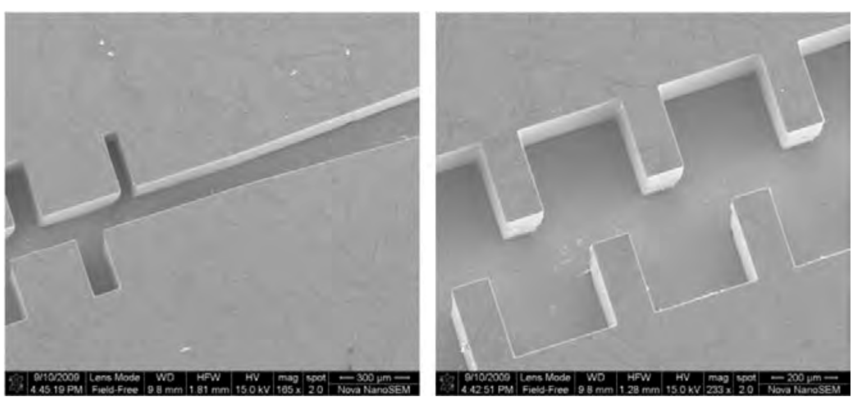

Fig. 10 SU8-LIGA fabricated TWT circuits

For metal deposition, two schemes available in the UC Davis class-100 clean room were used, namely (i) CHA E-beam evaporator; and (ii) CHA sputter coater. Fig. 11 shows the images for the deposition of copper using the e-beam evaporator while Fig. 12 shows the SEM images after copper sputter coating on the TWT circuits fabricated by SU8. A simple and effective test was conducted to check whether the metal has been deposited uniformly in the trenches, especially at the bottom curves. A simple tape mask was used and copper was deposited as only a strip across the circuit shown light brown in Fig. 13. The resistance meter was used to test if the metal coating is continuous across the circuit. It was determined that the metal coating worked out well on the exposed areas, but it was difficult for the metal coating to reach the bottom uniformly on these high aspect ratio structures. Hence, we continued on our work to produce the other approach of fully electroforming the circuit with mold present in place of the RF channel.

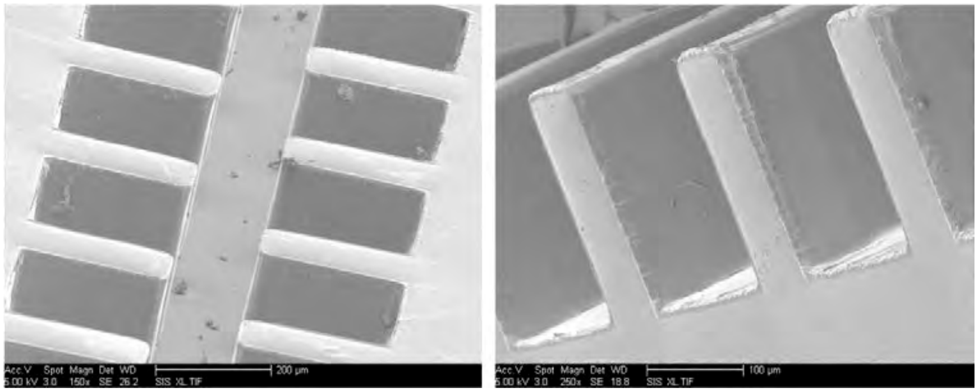

Fig. 11 SU-8 mold circuit with Cu coating by CHA E-beam evaporator

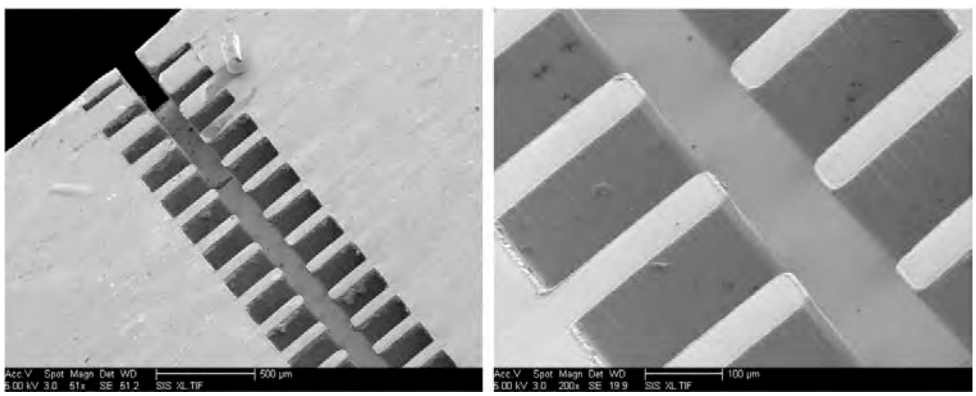

Fig. 12 SU-8 mold circuit with Cu coating using CHA-Sputter Coater

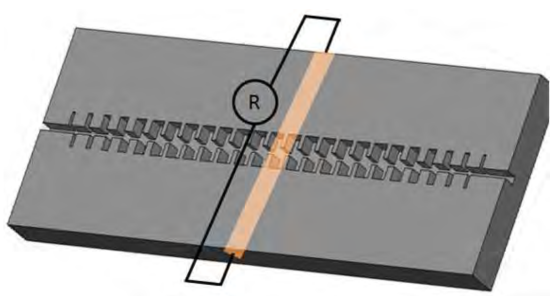

Fig. 13 Metal coating on a strip across the TWT structure and simple resistance continuity test for analyzing the effectiveness of metal coating in the bottom.

For the fully metalized/electroplated and polished circuit, the real challenge was to remove the SU8 mold that is known to be extremely stable after cross linking following UV exposure and development. To remove SU-8, we used a high temperature vacuum furnace under nitrogen atmosphere. The SEM analysis depicted in Fig. 14 (a, b) showed that in some parts of the TWT circuit, SU8 still remains in the bottom of the circuit, but in other areas SU8 was seen to be removed completely. We are currently working on optimizing the recipe for SU8 removal processing that has a potential for even better dimensionality and sustainability to the electroplating as compared to KMPR.

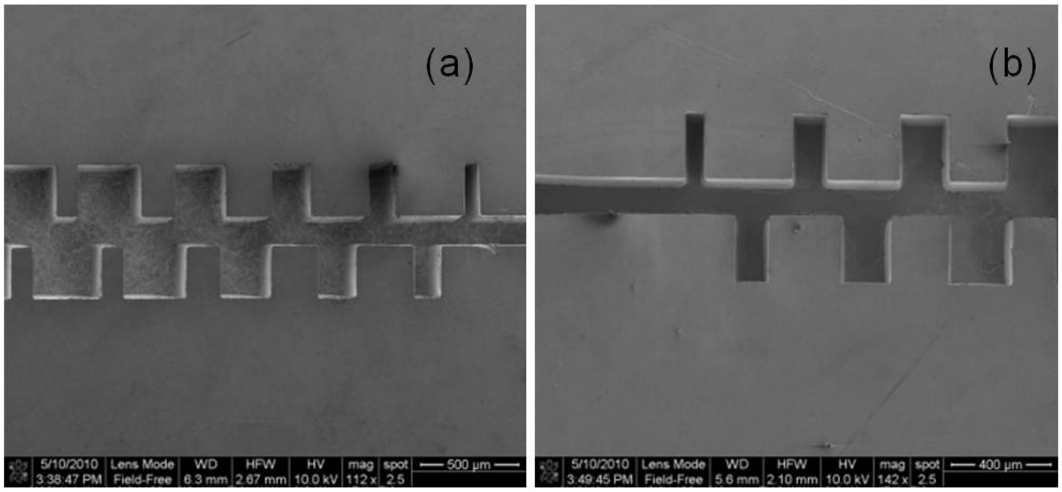

Fig. 14 Vacuum furnace burning of SU8 in nitrogen atmosphere

3.1.2 KMPR-LIGA

KMPR [51] negative tone photoresist is a chemically enhanced carboxylated epoxy resin comprising a photo-generated acid. This requires a post exposure bake to fully active the solidification process called cross-linking. For electroforming applications, this can withstand acidic solutions at relatively high temperatures compared to room temperature. A typical KMPR LIGA process flow chart is given in Fig. 15 (a-i). We worked on the specially fabricated 4 inch OFHC Cu wafers with highly flat ($\pm$ 0.5 μm) and polished surfaces. The process starts from spin coating (step a), soft bake, UV exposure, Post Exposure Bake (PEB), Electroplating, Lapping/Polishing and mold removal processing. Micro Chem reports [51] the process conditions for negative tone KMPR Photo-resist for thicknesses up to only about 120 *microns* at the highest viscosity product. For fabrication of 0.22 *THz* SBTWT micro-metallic circuits, we needed high aspect ratio structures with 75 *micron* smallest width of trench, and 385 *microns* depth. Consequently, we had to fully characterize the LIGA process for high thicknesses, stretching the limits beyond typical working scale in a class-100 clean room environment normally used by the semiconductor industry. We worked in great detail on each step meticulously and finally were able to fabricate fully metalized slow wave structure waveguides [3] for our 0.22 *THz* ultra wide band SBTWT.

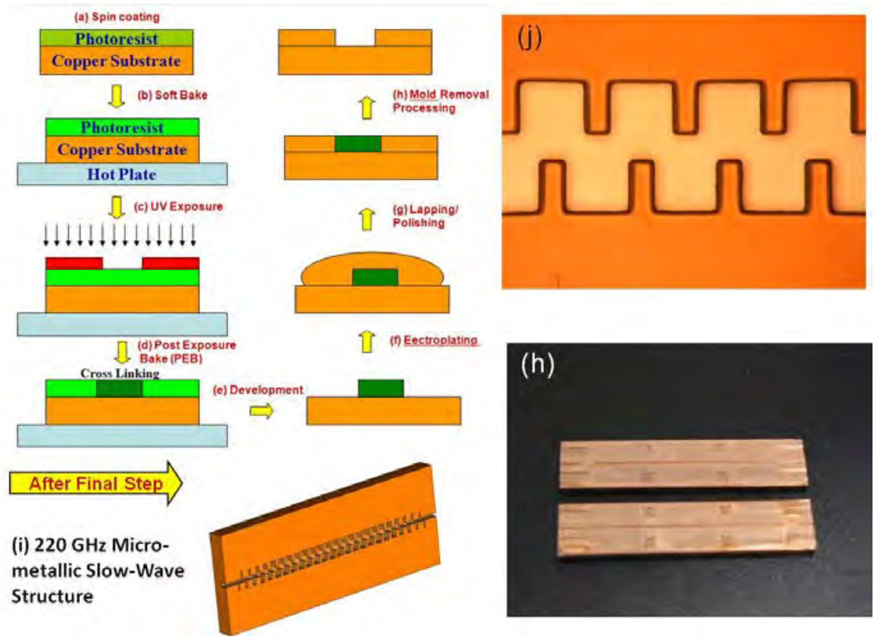

Fig. 15 (a-i) LIGA process flow chart (j) microscope image of KMPR mold on OFHC substrate (h) Digital Camera images of 0.22 *THz* SBTWT circuits after final mold removal processing.

Fig. 15 (j) shows the microscope image of the KMPR mold after the completion of the mold development step (e) in Fig. 15. The vanes are sharply defined with ~ 90^0 edges. For a thickness of ~ 400 μm in a single layer process, the optimum numbers for soft bake time is ~ 240 *min*, exposure energy of ~ 9500 mJ/cm^2, and post exposure bake of ~ 4 *min* at temperature 95^0C. The details can be found in our earlier work [2]. Fig. 15 (h) shows the finished SBTWT circuits after the mold removal processing step. Mold removal processing is also a very challenging step and debris that remains in the RF path can be seriously detrimental to the electromagnetic transmission. We also have optimized the KMPR mold removal process recipe that uses periodic DMSO and PG remover treatment at high temperature. EKC-8000 and sonic agitation at high temperature were also helpful, but that treatment shows more oxidation on the top copper surface. This can also be treated with a quick acidic mixture treatment for about ~ 30 *sec* and a thorough DI water rinse.

An extensive SEM Analysis was conducted to elucidate mold quality, mold removal efficiency, dimensional accuracy and wall verticality. Fig. 16 (a, b) shows the SEM images of the SBTWT circuits (with mold) with the couplers having slot spacing tapered at both ends for a broadband response. The smallest feature (75 μm wide and 385 μm wide) was successfully patterned with high dimensional definition. The samples were made in two batches and analyzed under SEM to verify the reproducibility of the SBTWT circuits using KMPR High Aspect Ratio Lithography (HARL) in a single process.

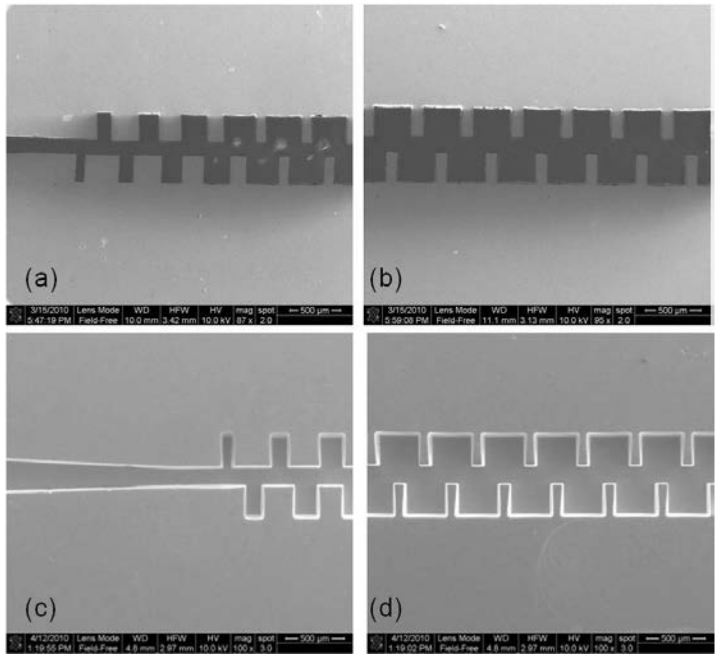

Fig. 16 (a, b) shows the SEM images before mold removal processing (c, d) shows the SEM images at 500 μm resolution of samples after mold removal processing.

As is observed in Fig. 16 (c, d), KMPR photoresist was completely removed from the trenches without the presence of flakes or debris inside. The dimensional accuracy was measured and summarized in the table below in Tab. 2. The maximum error of 5% was observed for the realization of the shortest cavity width of 75 μm with wall verticality of $90^0 \pm 1^0$. The surface roughness was also measured at different locations on the circuit using a 3D optical microscope and determined to range between 30 to 50 *nm* which is much less than the skin depth at 0.22 *THz* which is ~ 140 *nm*. The surface roughness should be held significantly below the skin depth at THz frequencies to keep the RF losses to an acceptable level. If a circuit has high surface roughness, this will translate into high electromagnetic radiation transmission losses which lead to reduced gain and output power of the vacuum electron device.

Tab. 2 Comparison of final SBTWT circuits fabricated by UV LIGA process and the design values.

	Design (μm)	Fabricated (μm)	Error (%)
Tunnel Width	150	145.82	2.78
Shortest Cavity Width	75	71.41	4.7
Second Cavity Width	135	136.48	1.096
Middle Cavity	345	335	2.89

The KMPR LIGA process was demonstrated clearly to be a viable MEMS fabrication technique for novel micro-scale vacuum electron devices at THz frequencies. The RF measurements/cold tests were also conducted on these samples that demonstrated promising results and are described in a later section.

3.2 Si-DRIE

DRIE (deep reactive ion etching) [2] was also used for the micro patterning of slow wave structures available in a class-100 clean room facility. A Si wafer was coated with a layer of negative tone photo-resist (~ 16 μm) on the top surface. The mask for the double vane staggered SBTWTA structure is created using the photolithography process. The Si is etched using Alcatel DRIE equipment in a Bosch process. This process is comprised of SF_6 etching and C_4F_8 passivation cycles that are repeated one after the other. The Si mold is then physically attached to the OFHC (Oxygen free high conductivity) copper for electroforming. For this high aspect ratio structure, it is very challenging to preserve the dimensional definition up to the bottom as can be seen in Fig. 17. We were able to optimize the DRIE process to produce a patterned Si-mold for ~ 400 μm tall and ~ 115 μm smallest features of our 0.22 *THz* SBTWT circuit. Fig. 18 shows the fully metalized TWT circuit using a Si-mold fabricated by the DRIE process.

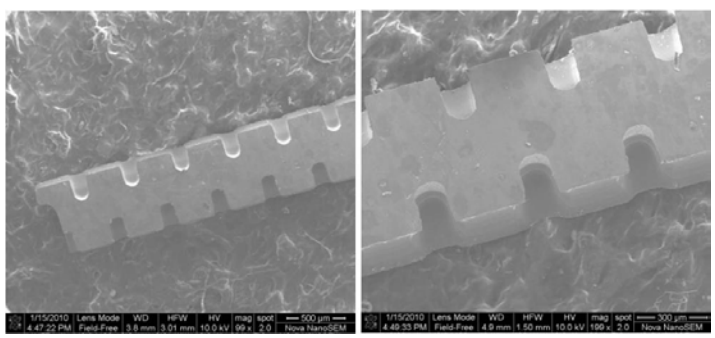

Fig. 17 SEM image of initial work on the Si-DRIE process.

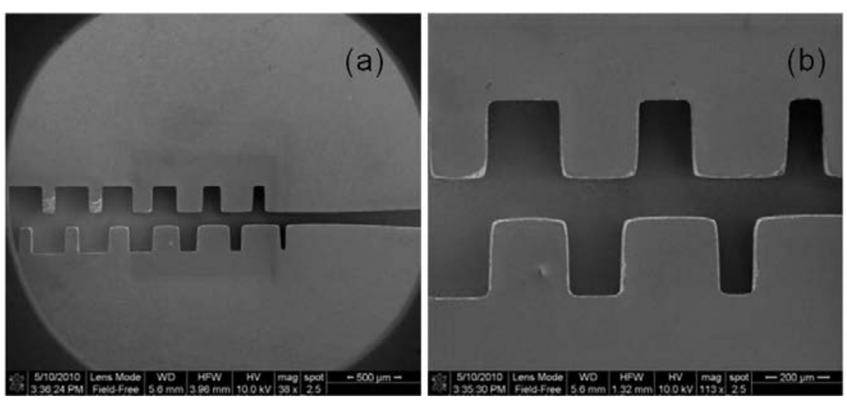

Fig. 18 Fully metalized double vane half staggered TWT structure using optimized DRIE molding process.

The dimensional deviations from the design values were measured to be ~ 3-5 μm. To improve the scalloping formed at the sidewalls of the Si-mold, a layer of SiO_2 approximately ~ 1 μm thick was formed using a high temperature O_2 furnace. This oxidized layer was subsequently stripped off to improve the side wall smoothness and reduce surface roughness. The typical surface roughness of ~ 30 *nm* was measured using a 3D microscope/AFM. We are currently trying to improve the adhesion of the Si-mold with the OFHC copper substrate to reduce the under-cut in the metalized structures. Furthermore, we are trying to incorporate a heat sink material beneath the Si-substrate to better remove the heat during the etching of the high aspect ratio structure to maintain the dimensional definition as we go deeper in the Si mold.

3.3 Nano CNC milling

As a first test, the 220 *GHz* wide bandwidth TWT structure was manufactured in aluminum using a nano CNC milling machine (Mori Seiki NN1000) designed by DTL. Aluminum was chosen for a first circuit prototype fabrication because it is much easier to machine than copper. The main issue when machining copper is that it is very ductile and “drags” with the tool not only causing heavy tool wear, but also leaving a prominent surface asperity. (UC Davis researchers were able to avoid these problems in their later tests with copper.) The circuit was fabricated in two halves cut along the “zero-current” plane. A 125 *micron* diameter tool was used for fabrication of this circuit, and the final depth of cut was 385 *microns* per half. The circuit was cold tested and found to exhibit > 10 *dB* loss (S_{21}) over ~ 50 *GHz* bandwidth that is quite high as compared to the simulation which predicted ~ 5 *dB* over 60 *GHz* bandwidth. After the initial tests, with the improvement in machining capability, availability of better tools, and using better conductivity material OFHC Cu, we obtained excellent results that are described in next section. The SEM image of the 0.22 *THz* TWTA circuit made in Aluminum is shown in Fig. 19.

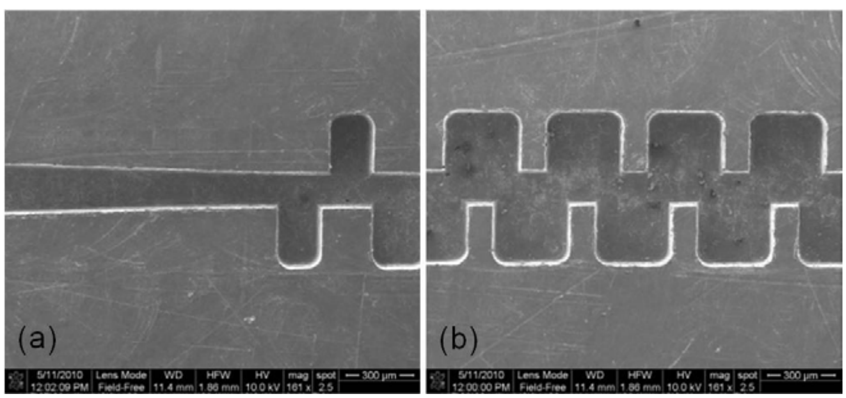

Fig. 19 0.22 *THz* slow wave circuit machined by nano CNC milling in Aluminum

4. RF Measurements

A scalar network analyzer setup was configured and is comprised of a BWO (Backward Wave Oscillator) operating in the frequency range of 165-270 *GHz*. Virginia Diodes, Inc. detectors were used for the sensitive detection of RF signals in this frequency range. The system was fully calibrated and tested for full operation before actual experimentation on UV-LIGA and Nano-machined fabricated 0.22 *THz* SBTWT circuits. 2D data interpolation schemes were used for an efficient and accurate data acquisition. The scalar network analyzer system was integrated to the PC for automated data acquisition using the NI LabView program. The SBTWT circuits were aligned precisely in a special fixture arrangement to minimize reflections. Fig. 20 below shows the RF measurement/cold test system employing the 165-270 *GHz* BWO.

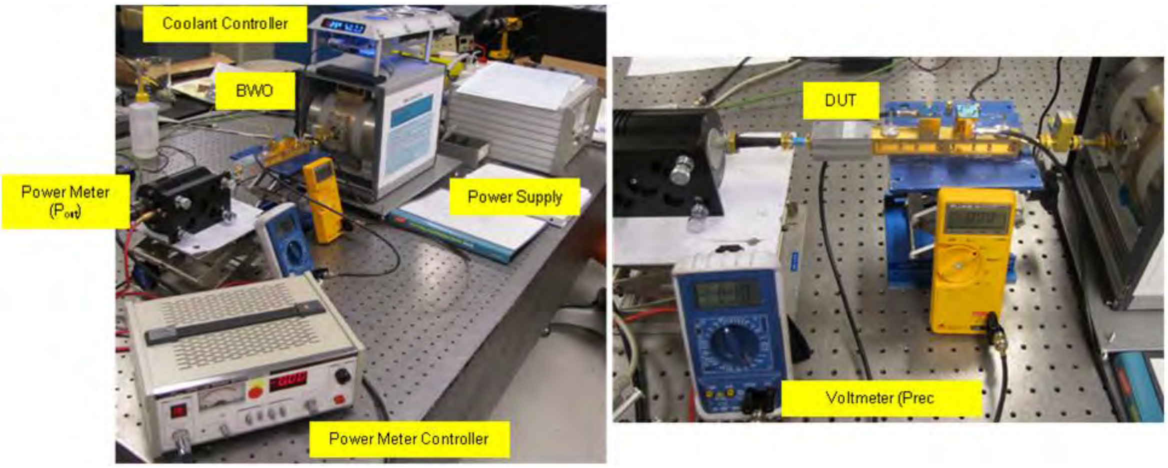

Fig. 20. Scalar Network Analyzer (RF measurement setup) for LIGA and Nano-machined TWT circuits

4.1 RF Analysis for LIGA fabricated TWTA circuit

The cold test results for the UV KMPR LIGA fabricated samples were quite impressive. The circuit exhibited transmission in the frequency range 214 *GHz*-266 *GHz* with insertion loss varying between 5 to 10 *dB* in general. Fig. 21(a) shows the comparison of the RF measurements and simulations for two different thicknesses of circuit halves, i.e 360 μm and 370 μm. As the figure demonstrates, the simulation prediction and measurement result match very well except that we observe a drop in S_{21} beyond 268 *GHz* which is attributed to the sharp reduction in the BWO output power at this frequency range. The return loss as depicted in Fig. 21 (b) was a little high and varied $\pm$ 3 *dB* around 7.5 *dB* as compared to the simulation that predicted ~ -15 *dB* in the passband. The peaks in transmission correlated well with the dips in return loss. The high return loss and the fluctuations are attributed to misalignments in the circuit and fixture. This pioneering effort for using KMPR in a UV LIGA process for VED fabrication on the THz scale proved completely viable and was demonstrated successfully by RF characterization experiments. We are currently doing experimental investigation for diffusion bonding the circuits prior to cold test that would further increase the transmission.

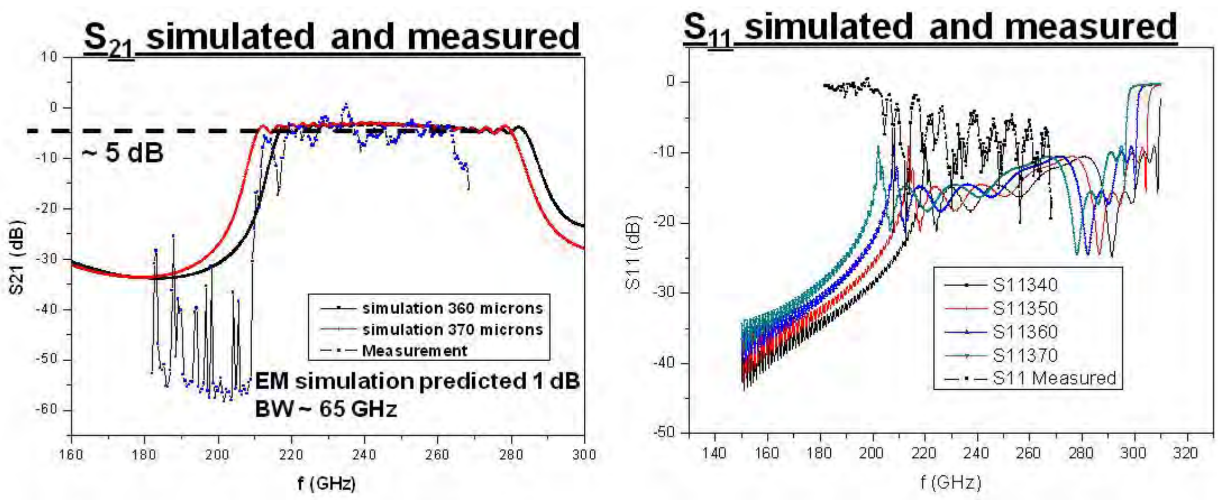

Fig. 21 0.22 *THz* TWT cold test/RF measurement and simulation comparison for different thicknesses of circuit halves.

4.2 RF Analysis/cold test for nano CNC fabricated TWTA circuit

With the same RF measurement setup described in the earlier section, nano machined SBTWT circuits were analyzed for RF transmission and reflection. Fig. 22 shows the comparison of simulation of the broadband couplers and measurement results. The broadband couplers have a gradual depth variation for impedance matching over a wide range of frequencies; this design was crucial for the efficient operation of the ultra wide-band SBTWTA designed at UCD. The simulation predicted a 1 *dB* bandwidth of ~ 70 *GHz*. The S_{21} measurement matched very well with simulation up to around 265 *GHz* beyond which the measurement setup was unable to take the data at the same power settings. The return loss remained a little higher than the simulation predicted around -10 *dB* in the pass band. This is attributed to the imperfections of the fixture assembly that holds the two halves of the SBTWT circuit together.

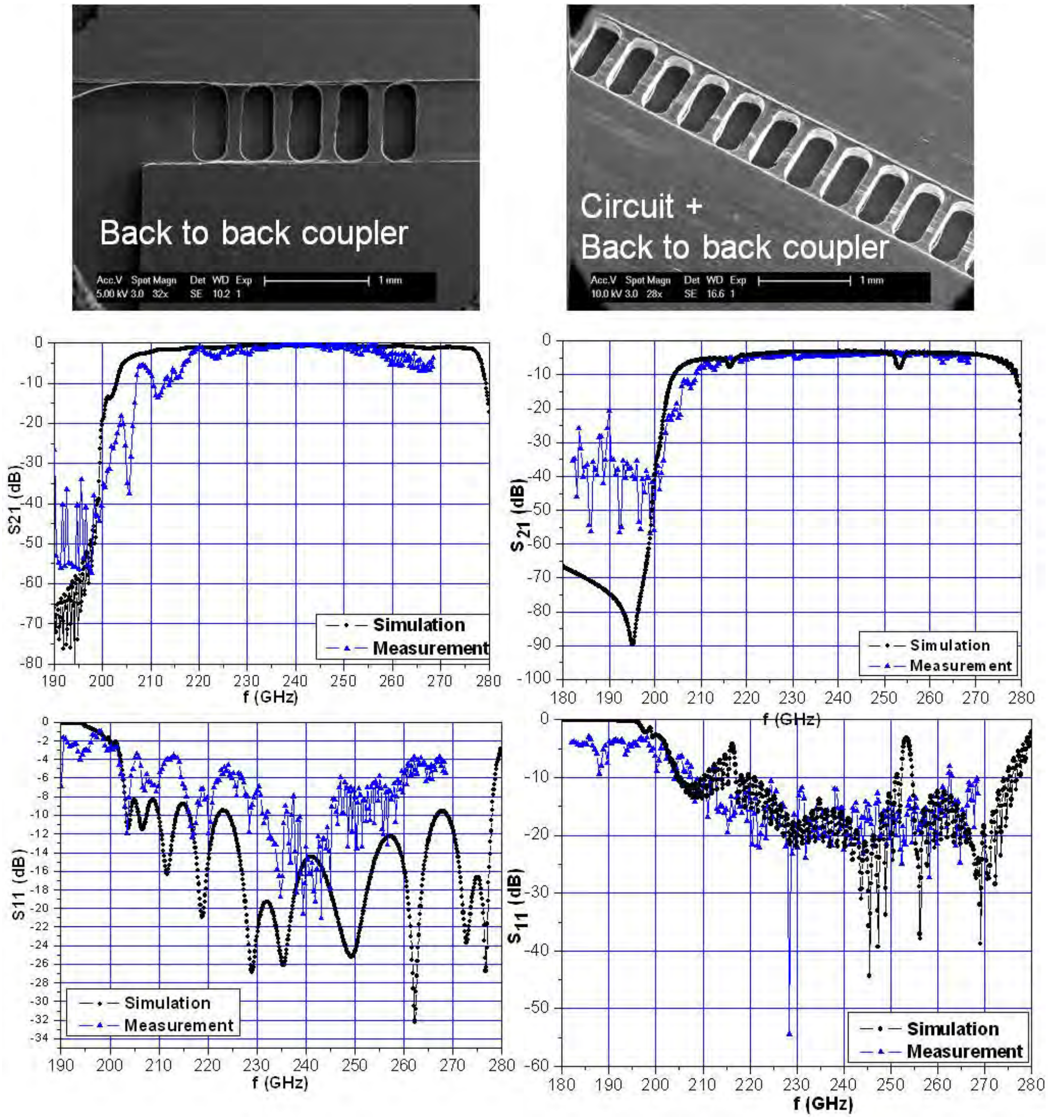

(a) (b)

Fig. 22 (a) SEM image of nano-machined broadband coupler and S-parameter comparison of simulation and RF measurements (b) SEM image of full TWT structure with couplers and S-parameters comparison of measured and simulated values

Fig. 22 shows the SEM image of the full model of 40 *mm* long nano-machined TWT circuit with the integrated broad-band couplers. The simulation of transmission (S_{21}) as shown in figure predicted a 1 *dB* band width greater than 60 *GHz*. The RF measurement agrees excellently with the 3D electromagnetic computational analysis. The return loss was seen to be matched with the computational predictions very well (< -10 *dB* in the passband). This was due to the fact that surface finish was improved by chemical cleaning (called bright dip) and an improved fixture setup to better hold the circuit.

5. Conclusions

We described our computational design, MEMS fabrication, and RF measurement analysis on a 0.22 *THz* sheet beam traveling wave tube amplifier. The idea behind this work is to be able to scale the vacuum integrated power amplifier technology into the THz range of the electromagnetic spectrum. This region of the electromagnetic spectrum 100 *GHz*-1 *THz* and beyond has the potential for fundamental research that can culminate into commercial devices and applications including security imaging and advanced communication systems. The utilization of MEMS based technologies that originally came about from the semi-conductor industry, has been an enabling factor in moving towards the goal of compact portable (?) device with practical power 0.01 *W*-tens of watts with an efficiency of > 1% and an instantaneous band width of 0.01.

Our numerical modeling analysis of the SBTWT yields a wide band velocity synchronism condition for n = 1 and $k_z d/\pi = 2.5$ that corresponds to an instantaneous band width of > 30 % with output power of > 50 *W*. . MAGIC and CST PIC codes match very well for the analysis of the output response of the SBTWT. The predicted output power of the circuit is ~ 150-300 *W* that corresponds to an intrinsic efficiency of ~ 3-6 % with a gain of ~ 35-37 *dB* for an input drive of 50 *mW*. The efficiency of the TWTA for actual device applications can be as high as ~ 12% by employing depressed collector with a nominal recovery efficiency of ~ 50%. The peak in the P_{out} versus frequency curve is being studied in more detail to preclude any high order parasitic oscillations. For a realistic compact device, we described our work on the PPM based sheet beam focusing structure employing $SmCo_6$ and NdFeB permanent magnets. The optimized structure could focus the sheet beam through transport in a beam tunnel of 770 *μm* by 150 *μm* dimensions with an efficiency of ~ 80 % for a stack to stack spacing of ~ 2.6 *mm* and ~ 73% for an increased stack spacing of ~ 4 *mm* to accommodate the vacuum ports in the narrow dimension. NdFeB permanent magnets with high remanence magnetization (Br ~ 1.4 T) were used for the latter case. Using the NdFeB PPM B-field in the PIC simulations predicted an output power of ~ 75 *W* and gain ~ 17 *dB* for an input drive of ~ 1*W* at 0.22 *THz* and transmitted current of ~ 190 *mA*. For MEMS fabrication of SBTWT slow wave structures that are double vane half period staggered gratings, we considered different schemes namely: (a) UV LIGA SU-8 and KMPR; (b) Si DRIE; and (c) Nano-machining/nano CNC milling. We characterized the entire LIGA process and demonstrated fabricated circuits within 3 - 5 *μm* error and surface roughness of 30-80 *nm*. SU-8 removal has also been investigated using burning in a furnace with nitrogen. SU-8 was also used to fabricate the circuits and metal coating schemes were employed using a CHA e-beam evaporator and CHA sputter coater. A simple continuity test by coating only a thin metal strip showed that metal could not be deposited very well in the bottom. However, our other approach of complete electro-forming the KMPR molds and doing complete mold removal processing as a last step gave very promising results as shown by SEM and 3D microscope analysis. The maximum error in the fully metalized KMPR LIGA circuits was 4.7 *μm* for the narrowest cavity while the surface roughness stayed far below the skin depth (140 *nm* at 0.22 *THz*), i.e. ~ 50 *nm*. RF measurements on the LIGA and nano-machined circuits demonstrated excellent agreement with the simulation predictions. The S_{21} value remained around ~ 5 *dB* in the passband of 214-266 *GHz* while S_{11}varied around -10 *dB*. The return loss and surface roughness was even better for the nano-machined circuits. The results for the full SBTWT model with broad band couplers also showed excellent agreement with the simulation.

We are currently preparing for the exploratory hot test employing the MEMS fabricated circuits in a fixture assembly with the electron beam assembly and magnetic focusing structure. We hope that after this proof of concept experiment we can scale this SBTWTA design to even higher frequencies to potentially fill the so called THz gap.

Acknowledgements:

The authors would like to acknowledge the help rendered by Northern California Nano-Technology Centre (NCNC), UC Davis. We like to acknowledge useful discussion and help by Dr. Frank Yaghmaie, Mr. Robert Prohaska and Mr. Dan Haskell of NCNC for our work on MEMS fabrication and metal coating techniques.

We also would like to thank Ph.D student Mr. Alex Spear for his help in setting up the automatic data acquisition scalar network analyzer system employing BWO.

We also would like to thank Mr. Chris Robertson for working with the improvement of home-made electroplating system.

We like to thank Dr. Ali Farvid, metal finishing shop, SLAC for his help in the characterization of electroplating solutions and sharing useful ideas on metal finishing and quality improvement.

This work is supported by the HiFIVE (High Frequency Integrated Vacuum Electronics) program of DARPA (Defense Advanced Projects Agency), Grant No. G8U543366, through a subcontract with Teledyne Scientific.

References

[1] J. E. Atkinson, D. D. Gajaria, T. J. Grant, T. Kimura, B. C. Stockwell, M. Field, R. J. Borwick, B. Brar, and J. A. Pasour, "8.3: A high aspect ratio, high current density sheet beam electron gun", *Vacuum Electronics Conference (IVEC), 2010 IEEE International*, 97-98. (2010).

[2] Shin Young-Min, D. Gamzina, L. R. Barnett, F. Yaghmaie, A. Baig, and N. C. Luhmann, "UV Lithography and Molding Fabrication of Ultrathick Micrometallic Structures Using a KMPR Photoresist", *Microelectromechanical Systems, Journal of,* 19, 683-689, (2010).

[3] A. Baig, D. Gamzina, M. Johnson, C. W. Domier, A. Spear, L. R. Barnett, N. C. Luhmann, and Shin Young-Min, "Experimental characterization of LIGA fabricated 0.22 THz TWT circuits", *Vacuum Electronics Conference (IVEC), 2011 IEEE International*, 275-276, (2011).

[4] Shin Young-Min, A. Baig, A. Spear, Zhao Jinfeng, D. Gamzina, C. W. Domier, and N. C. Luhmann, "MEMS fabrications of broadband epsilon negative (ENG) metamaterial electronic circuit for 0.22 THz sheet beam TWT application", *Infrared Millimeter and Terahertz Waves (IRMMW-THz), 2010 35th International Conference on*, 1-2, (2010).

[5] Young-Min Shin, Larry R. Barnett, Diana Gamzina, Jr Neville C. Luhmann, Mark Field, and Robert Borwick, "Terahertz vacuum electronic circuits fabricated by UV lithographic molding and deep reactive ion etching", *Applied Physics Letters,* 95, 181505-3, (2009).

[6] D. Gamzina, R. Barchfeld, L. R. Barnett, N. C. Luhmann, and Shin Young-Min, "Nano CNC milling technology for terahertz vacuum electronic devices", *Vacuum Electronics Conference (IVEC), 2011 IEEE International*, 345-346, (2011).

[7] Gwyn P Williams, "Filling the THz gap - high power sources and applications", *Rep. Prog. Phys.,* 69, 301-326, (2006).

[8] Peter H. Siegel, "Terahertz Technology", *IEEE Transactions on Microwave theory and Techniques,* 50, (2002).

[9] Chen Xiaodong and Li Daohui, "High power Terahertz generation by using vacuum electronic technology", *Broadband Network & Multimedia Technology, 2009. IC-BNMT '09. 2nd IEEE International Conference* , 921-924, (2009).

[10] John H. Booske, "Plasma physics and related challenges of millimeter-wave-to-terahertz and high power microwave generation", *Physics of Plasmas,* 15, 055502-16, (2008).

[11] Goutam. Chattopadhyay, Kem. Cooper, Robert. Dengler, Tomas E. Bryllert., Erich Schlecht, Anders Skalare, Imran Mehdi, and Peter H. Siegel, "A 600 GHz Imaging Radar for Contraband Detection", *19th International Symposium on Space Terahertz Technology*, Groningen, 28-30, (2008).

[12] R. Appleby and H. B. Wallace, "Standoff Detection of Weapons and Contraband in the 100 GHz to 1 THz Region", *IEEE Transactions on Antennas and Propagation,* 55, 2944, (2007).

[13] A. Giles Davies, Andrew D. Burnett, Wenhui Fan, Edmund H. Linfield, and John E. Cunningham, "Terahertz spectroscopy of explosives and drugs", *Materials Today,* 11, 18-26, (2008).

[14] Masayoshi Tonouchi, "Cutting-edge terahertz technology," *Nat Photon,* 1, 97-105, (2007).

[15] Larry Yujiri, Merit Shoucri, and Philip Moffa, "Passive Millimeter-Wave Imaging", *IEEE Microwave Magazine,* 39-50, (2003).

[16] Neville C. Luhmann Robert J Barker, John H. Booske, Gregory S. Nusinovich, "Modern Microwave and Millimeter-Wave Power Electronics", IEEE/Wiley, (2005).

[17] T. W. Crowe, D. W. Porterfield, J. L. Hesler, W. L. Bishop, and D. S. and Hui Kurtz, K., "Terahertz technology for imaging and spectroscopy", *Proceedings of the SPIE - The International Society for Optical Engineering*, 6212, (2006)

[18] B. S. Williams, S. Kumar, Q. Hu, and J.L Reno, "High-Power terahertz quantum-cascade lasers", *Electronics Letters,* 42, 89-90, (2006).

[19] V. P. Bolotin, V. S. Cherkassky, E. N. Chesnokov, B. A. Knyazev, E. I. Kolobanov, V. V. Kotenkov, A. S. Kozlov, V. V. Kubarev, G. N. Kulipanov, A. N. Matveenko, L. E. Medvedev, S. V. Miginsky, L. A. Mironenko, A. D. Oreshkov, V. K. Ovchar, A. K. Petrov, V. M. Popik, P. D. Rudych, T. V. Salikova, S. S. Serednyakov, A. N. Skrinsky, O. A. Shevchenko, M. A. Scheglov, M. B. Taraban, N. A. Vinokurov, and N. S. Zaigraeva, "Novosibirsk terahertz free electron laser: status and survey of experimental results", *Infrared and Millimeter Waves and 13th International Conference on Terahertz Electronics, 2005. IRMMW-THz 2005. The Joint 30th International Conference on*, 495-496, 2, (2005).

[20] Mark Sherwin, "Applied physics: Terahertz power", *Nature,* 420, 131-133, (2002).

[21] V.A. Flyagin, A. G. Luchinin, and G. S. Nusinovich, "Sub mmwave Gyrotrons - Theory and Experiment", *Int. J Infrared Millimeter Waves,* 4, 629, (1983).

[22] M. C. Lin, P. H. Stoltz, D. N. Smithe, H. Song, S. J. Kim, S. H. Jang, G. W. Choi, and J. J. Choi, "Modeling of multistage depressed collectors using a 3D conformal finite-difference time-domain particle-in-cell code", *Plasma Science, 2010 Abstracts IEEE International Conference on*, 1-1, (2010).

[23] J. X. Qiu, B. Levush, J. Pasour, A. Katz, C. M. Armstrong, D. R. Whaley, J. Tucek, K. Kreischer, and D. Gallagher, "Vacuum Tube Amplifiers", *IEEE Microwave Magazine,* 38-51, (2009).

[24] R. H. Abrams, B. Levush, A. A. Mondelli, and R. K. Parker, "Vacuum Electronics for the 21st century", *IEEE Microwave Magazine,* 61-72, (2001).

[25] Brian. Coaker and Tony. Challis, "Traveling Wave Tubes: Modern Devices and Contemporary Applications", *Microwave Journal,* 32-46, (2008).

[26] J. H. Booske, R. J. Dobbs, C. D. Joye, C. L. Kory, G. R. Neil, Park Gun-Sik, Park Jaehun, and R. J. Temkin, "Vacuum Electronic High Power Terahertz Sources", *Terahertz Science and Technology, IEEE Transactions on,* .1, 54-75, (2011).

[27] B. E. Carlsten, S. J. Russell, L. M. Earley, F. L. Krawczyk, J. M. Potter, P. Ferguson, and S. Humphries, Jr., "Technology Development for a mm-Wave Sheet Beam Traveling-Wave Tube", *IEEE Transactions on Plasma Science,* 33, 85-93, (2005).

[28] Young-Min Shin and Larry R. Barnett, "Intense wideband terahertz amplification using phase shifted periodic electron-plasmon coupling", *Applied Physics Letters,* 92, 091501-3, (2008).

[29] Young-Min Shin, Larry R. Barnett, and Jr Neville C. Luhmann, "Strongly confined plasmonic wave propagation through an ultrawideband staggered double grating waveguide", *Applied Physics Letters,* 93, 221504-3, (2008).

[30] Shin Young-Min, L. R. Barnett, and N. C. Luhmann, "Phase-Shifted Traveling-Wave-Tube Circuit for Ultrawideband High-Power Submillimeter-Wave Generation", *Electron Devices, IEEE Transactions on,* 56, 706-712, (2009).

[31] K. Mizuno and S. Ono, *Journal of Applied Physics,* 46, (1975).

[32] M. I. Lopin, A. S. Pobedonostsev, and B. V. Sazonov, "High-power multiple beam TWTs and the TWT-based amplifying chains", *Microwave Symposium Digest, 1992., IEEE MTT-S International*, 145-146, 1, (1992).

[33] G. Scheitrum, "Design and Construction of a W-Band Sheet Beam Klystron", *7th Workshop on High Energy Density and High Power RF*, Kalamta, Greece, (2005).

[34] John H. Booske, W. Destler, Z. Segalov, D. Radack, E. Rosenbury, J. Rodgers, T. Antonsen, V. Granatstein, and I. Mayergoyz, "Propagation of wiggler focused relativistic sheet electron beams", *J Appl. Phys.,* 64, 6 - 11, (1988).

[35] J. H. Booske, Brian D. Mcvey, and Thomas M. Antonsen Jr., "Stability and confinement of non-relativistic sheet electron beams with periodic cusped magnetic focusing", *J. Appl. Phys.,* 73, 4140 - 4155, (1993).

[36] Jian-Xun Wang, Larry R. Barnett, Jr Neville C. Luhmann, Young-Min Shin, and Stanley Humphries, "Electron beam transport analysis of W-band sheet beam klystron", *Physics of Plasmas,* 17, 043111-11, (2010).

[37] A. Baig, Wang Jian-Xun, L. R. Barnett, N. Luhmann, and Shin Young-Min, "Beam transport modeling of PPM focused THz sheet beam TWT circuit", *Vacuum Electronics Conference (IVEC), 2011 IEEE International*, 351-352, (2011).

[38] Diana. Gamzina, A. Spear, Larry R. Barnett, and N. C. Luhmann, "Terahertz Sheet Beam Gun Analyzer", *IEEE International Vacuum Electronics Conference,* 99-100, (2010).

[39] J. H. Booske R. J Barker, N. C. Luhmann, and G. S. Nusinovich, "Modern Microwave and Millimeter-Wave Power Electronics", (2005).

[40] J. R. Pierce, "Traveling Wave Tubes", (1950).

[41] A. S. Gilmour, "Principles of Traveling Wave Tubes", (1994).

[42] Han Seong-Tae, "Investigations on a Microfabricated FWTWT Oscillator," *IEEE transactions on Electron Devices,* 52, (2005).

[43] Shin Young-Min, Park Gun-Sik, G. P. Scheitrum, and B. Arfin, "Novel Coupled Cavity TWT Structure Using Two-Step LIGA Fabrication", *IEEE Transactions on Plasma Science,* 31, (2003).

[44] R. Lawrence Ives, "Microfabrication of High Frequency Vacuum Electron Devices," *IEEE Transactions on Plasma Science,* 32, 1277-1291, (2004).

[45] M R Lueck, D. M Malta, Gilchrist K. H., C. L. Kory, C. T. Mearini, and J. A. Dayton, "Microfabrication of diamonf-based slow wave circuits for mm-wave and THz vacuum electronics sources", *J. Micromech. Microeng. ,* 21, 1-7, (2011).

[46] Shin Young-Min, L. R. Barnett, and N. C. Luhmann, "Numerical and experimental design study of quasi-optical multi-gap output cavity for W-band sheet beam klystron (WSBK)", *Vacuum Electronics Conference, 2009. IVEC '09. IEEE International*, 530-532, (2009)

[47] G. Scheitrum, G. Caryotakis, A. Burke, A. Jensen, E. Jongewaard, M. Neubauer, R. Phillips, and R. Steele, "W-band Sheet Beam Klystron Research at SLAC", *Vacuum Electronics Conference, 2006 held Jointly with 2006 IEEE International Vacuum Electron Sources., IEEE International*, 481-482, (2006).

[48] G. Scheitrum, G. Caryotakis, A. Jensen, A. Burke, A. Haase, E. Jongewaard, M. Neubauer, and B. Steele, "Fabrication and Testing of a W-band Sheet Beam Klystron", *Vacuum Electronics Conference, 2007. IVEC '07. IEEE International*, pp. 1-2, (2007).

[49] Young-Min Shin, Jin-Kyu So, Seong-Tae Han, Kyu-Ha Jang, Gun-Sik Park, Jong-Hyun Kim, and Suk-Sang Chang, "Microfabrication of millimeter wave vacuum electron devices by two-step deep-etch x-ray lithography", *Applied Physics Letters,* 88, 091916-3, (2006).

[50] Microchem SU-8.

[51] Microchem KMPR.

[52] Colin D Joye, J. P. Calame, M. Garven, and B. Levush, "UV LIGA microfabrication of 220 GHz sheet beam amplifier gratings with SU-8 photoresists", *J. Micromech. Microeng.,* 20, (2010).

[53] C. Cremers, F. Bouamrane, L. Singleton, and R. Schenk, "SU-8 for resist material for deep X-ray lithography", *Microsyst. Technology,* 7, 11-16, (2001).

[54] Llobera Andreu, Seidemann Volker, A. Plaza Jos, Cadarso Vctor Javier, and Buttgenbach Stephanus, "SU-8 optical acceleromaters", *J. Microelectromech. Syst.,* 16, 11-16, (2007).

[55] Paul M. Dentinger, W. Miles Clift, and Steven H. Goods, "Removal of SU-8 photoresist for thick film applications", *Microelectronic Engineering,* 61-62, 993-1000, (2002).

[56] C. D. Joye, J. P. Calame, K. T. Nguyen, D. Pershing, P. B. Larsen, M. Garven, Park Doewon, R. Bass, and B. Levush, "Microfabrication of wideband distributed beam amplifiers at 220 GHz", *Vacuum Electronics Conference (IVEC), 2011 IEEE International*, 343-344, (2011).

[57] C. D. Joye, J. P. Calame, M. Garven, D. Park, R. Bass, and B. Levush, "UV-LIGA and DRIE grating microfabrication and testing for sheet beam amplifiers at 220 GHz", *Infrared Millimeter and Terahertz Waves (IRMMW-THz), 2010 35th International Conference on*, 1-2, (2010).